Experimental Neurology 321 (2019) 113031

Contents lists available at ScienceDirect

Experimental Neurology

journal homepage: www.elsevier.com/locate/yexnr

Research paper

A neutral lipid-enriched diet improves myelination and alleviates peripheral nerve pathology in neuropathic mice

Ye Zhou[a], Hannah Bazick[a], Joshua R. Miles[c], Alexander I. Fethiere[a], Mohammed Omar Al Salihi[a], Sergio Fazio[c], Hagai Tavori[c], Lucia Notterpek[a,b,*]

[a] Department of Neuroscience, College of Medicine, McKnight Brain Institute, University of Florida, Gainesville, FL 32610, USA
[b] Department of Neurology, College of Medicine, McKnight Brain Institute, University of Florida, Gainesville, FL 32610, USA
[c] Department of Medicine, Knight Cardiovascular Institute, Center for Preventive Cardiology, Oregon Health & Science University, Portland, OR 97239, USA

ARTICLE INFO

Keywords:
Peripheral neuropathy
Lipid-enriched diet
Trembler J mice
Peripheral myelin protein 22
Macrophage
Cholesterol

ABSTRACT

Charcot-Marie-Tooth (CMT) diseases comprise a genetically heterogeneous group of hereditary peripheral neuropathies. Trembler J (TrJ) mice carry a spontaneous mutation in peripheral myelin protein 22 (PMP22) and model early-onset, severe CMT type 1E disease. Recent studies indicate that phospholipid substitution, or cholesterol-enriched diet, benefit myelinated nerves, however such interventions have not been tested in early-onset dysmyelinating neuropathies. Here, we examined the lipid profile of peripheral nerves from 6-month-old TrJ mice with advanced neuropathy and tested the impact of a 6-week-long neutral lipid-enriched high-fat diet (HFD) on neuropathy progression in young, newly-weaned mice. Oil Red O staining showed pronounced neutral lipid accumulation in nerves from 6-month-old TrJ mice, along with elevated levels of key cholesterol and triglyceride transport proteins including apoE, LRP1 and ABCA1, compared with wild type (Wt). In young mice, the short-term HFD intervention increased serum cholesterol levels without impacting triglycerides, or body and liver weights. Tissue samples from neuropathic TrJ mice showed improvements in the maintenance of myelinated axons after the 6-week-long dietary intervention, and this effect was evident both in the sciatic and phrenic nerves. Concomitantly, aberrant Schwann cell proliferation was attenuated, as detected by reduction in mitotic markers and in c-Jun expression. Nerves from HFD-fed TrJ mice contained fewer macrophages, with a normalized count of CD11b + cells. In addition, we detected an increase in neutral lipids in the nerve endoneurium and a trend toward normalization of apoE, LRP1, and ABCA1 expression after the HFD feeding. Together, these results demonstrate the beneficial influence of a short-term neutral lipid-enriched diet on neuropathy progression in young TrJ mice and support further work in investigating the potential benefits of dietary lipids on hereditary neuropathies.

1. Introduction

Charcot-Marie-Tooth (CMT) diseases represent a heterogeneous group of progressive hereditary peripheral neuropathies. It is estimated that in ~60% to nearly 90% of patients the primary defect involves myelin dysfunction due to mutations in Schwann cell proteins, such as peripheral myelin protein 22 (PMP22) (DiVincenzo et al., 2014; Ekins et al., 2015; Fridman et al., 2015). So far, > 45 missense mutations in PMP22 have been identified, phenotypically ranging from mild compression-induced neuropathies to severe early-onset diseases (Li et al., 2013). Trembler J (TrJ) mice carry a spontaneous Leu16Pro substitution in the first transmembrane domain of PMP22, which is identical to a mutation in humans with early-onset severe neuropathy (Suter et al., 1992a). The abnormal L16P-PMP22 is retained in the intermediate Golgi compartment, triggering ER stress and activation of the autophagy-lysosomal pathway (Notterpek et al., 1997; Tobler et al., 1999; Fortun et al., 2003). Through heterodimer formation, L16P-PMP22 impairs the processing of WT-PMP22, and thus leads to a toxic "gain-of-function" phenotype (D'Urso et al., 1998; Tobler et al., 1999). Nerves from heterozygous TrJ mice show hypomyelination during early postnatal development, with pronounced demyelination and axonal atrophy by 6-month of age (Notterpek et al., 1997). Affected nerves demonstrate Schwann cell hypertrophy, macrophage infiltration, which mimic the neuropathology of CMT1E and Dejerine-Sottas disease (Notterpek et al., 1997; Notterpek and Tolwani, 1999; Misko et al., 2002). The TrJ mutation in the homozygous genotype is lethal around weaning age,

* Corresponding author at: 1149 S. Newell Dr., PO Box 100244, Gainesville, FL 32611, USA.
E-mail address: Notterpek@ufl.edu (L. Notterpek).

https://doi.org/10.1016/j.expneurol.2019.113031
Received 23 March 2019; Received in revised form 27 July 2019; Accepted 2 August 2019
Available online 03 August 2019

possibly due to dysfunctional neuromuscular junctions and subsequent paralysis (Notterpek et al., 1997; Scurry et al., 2016).

Myelin is fundamental in facilitating the conduction of electrical impulses in the nervous system. Similar to other biological membranes, myelin contains high levels of lipids, accounting for 70% of its total dry weight (Jackman et al., 2009; Brady et al., 2011). Phospholipids are most abundant in peripheral nerves and are required for myelin formation (Jackman et al., 2009; Brady et al., 2011). In addition to polar phospholipids, non-polar neutral lipids such as cholesterol esters and triglycerides are also abundant (Berry et al., 1965). Indeed, cholesterol constitutes ~26% of total lipids and is essential for myelin development and maintenance (Saher et al., 2005; Jackman et al., 2009; Saher et al., 2009; Brady et al., 2011). When genes controlling cholesterol or fatty acid synthesis are mutated in Schwann cells, affected mice develop abnormally myelinated peripheral nerves (Saher et al., 2009; Cermenati et al., 2015; Montani et al., 2018). In accordance, in CMT1A animals with PMP22 overexpression, genes related to lipid synthesis are significantly down-regulated (Vigo et al., 2005; Fledrich et al., 2012), while in PMP22-deficent mice genes and proteins related to cholesterol transport are induced (Zhou et al., 2019). In sciatic nerves of Trembler (Tr) mice, carrying a PMP22 point mutation at Glycine 150 to Aspartic acid (Suter et al., 1992b), ketone body incorporation for lipid synthesis is decreased (Clouet and Bourre, 1988). It was previously reported that while most lipids are significantly reduced in nerves from Tr mice, the levels of cholesterol esters are increased compared to normal (Larrouquere-Regnier et al., 1979; Juguelin et al., 1986). Detailed studies on lipid metabolism in nerves from TrJ mice have not been performed.

Although nerve lipids are normally produced in situ (Jurevics and Morell, 1994; Schmitt et al., 2015), peripheral nerves can be impacted by exogenous lipids from plasma. Under long-term systemic hyperlipidemic conditions, such as in diabetes, axons of peripheral nerves may be affected and damaged (Xu et al., 2014; Feldman et al., 2017). Fatty acid transport proteins, found in the myelin sheath, can incorporate long-chain fatty acids and influence axonal biology (Feldman et al., 2017). In demyelinated CNS lesions, exogenous dietary cholesterol was shown to support oligodendrocyte precursor differentiation and provide permissive environment for myelin repair (Berghoff et al., 2017). In the PNS, a phospholipid-enriched diet rescued myelinated axons and ameliorated neuropathic symptoms in CMT1A rats (Fledrich et al., 2018).

Here, we examined the involvement of lipid metabolism in symptomatic TrJ neuropathic nerves, and investigated the influence of a neutral lipid-enriched diet on the pathogenesis of the neuropathy in newly-weaned, 3-week-old mice. After a 6-week-long high-fat diet (HFD) intervention, we observed improved myelination, with reduced cell proliferation and fewer macrophages in TrJ neuropathic nerves. This short-term HFD intervention had no detrimental effects on nerves in Wt mice.

2. Materials and methods

2.1. Mice, diet and experimental design

Breeding colonies of wild type (Wt) and heterozygous Trembler J (TrJ) mice on the C57BL/6 background were purchased from the Jackson Laboratory (Bar Harbor, ME) and housed in pathogen-free facilities at the University of Florida McKnight Brain Institute. The use of animals for these studies was approved by the Institutional Animal Care and Use Committee (IACUC) of the University of Florida.

We determined the genotype of each animal by PCR using genomic DNA isolated from tail biopsies (Notterpek et al., 1997). At 3 weeks of age, male and female Wt and neuropathic TrJ mice were randomly assigned to a 6-week-long control chow (CD) (2018, Envigo, Madison, Wisconsin) or a neutral lipid-enriched, high-fat diet (HFD) (88,137, Envigo). The HFD provides 42% of calories from fat, compared with 18% in the CD. Detailed information on the diets is shown in Table 1. Before sacrifice and tissue collection, mice were fasted for 4–6 h and the body weight was measured. After euthanasia, blood was collected for serum isolation, and the remaining blood was flushed out at low pressure via transcardial perfusion using cold phosphate buffered saline (PBS). Subsequently, the whole liver and the sciatic nerves were collected. The effects of HFD feeding were similar between male and female mice, thus the results include data from both sexes combined. In total, we used 66, 3-week-old TrJ mice for the diet intervention studies.

Table 1
Lipid and calorie information of control diet (CD) (2018, Envigo) and high-fat diet (HFD) (88,137, Envigo) used in the study. N/A: not available.

	Control diet (CD)	High-fat diet (HFD)
Cholesterol	N/A	0.2%
Triglycerides	6.2%	20.8%
Saturated	0.9%	12.8%
Monounsaturated	1.3%	5.6%
Polyunsaturated	3.4%	1.0%
Phospholipids	N/A	< 0.02%
Free fatty acids	N/A	< 0.06%
Calories	3.1 kcal/g	4.5 kcal/g
Calories from carbohydrates	58.0%	42.7%
Calories from protein	24.0%	15.2%
Calories from Fat	18.0%	42.0%

2.2. Oil Red O staining

Frozen sciatic nerves were sliced at 20 μm thickness and fixed in 4% paraformaldehyde (PFA) for 30 min. Freshly-frozen livers were sectioned at 8 μm thickness and fixed in 10% formalin for 15 min. Sections were immersed in 0.5% Oil Red O solution in propylene glycol (Sigma, St. Louis, MO) for 10 min at 60 °C. After differentiation in 85% propylene glycol, samples were counterstained with Mayer's Hematoxylin (Sigma) and mounted with a glycerol-based mounting media (Thermo Fisher, Waltham, MA). Images were digitally captured using an Olympus BX43 upright microscope outfitted with an Olympus DP80 camera. Lipid particle density was quantified using the NIH Image J software. Briefly, a colour threshold was selected, and lipid particles with an area size > 0.15 μm^2 were counted automatically by the software.

2.3. Western-blotting

Frozen sciatic nerves were homogenized in modified radioimmunoprecipitation assay (RIPA) buffer (25 mM Tris, 150 mM NaCl, pH: 8.0, 2% SDS, 0.5% sodium deoxycholate, 1% TritonX-100) supplemented with complete protease (Roche, Basel, Switzerland) and phosphatase (Sigma) inhibitors. Equal amounts of protein were separated on sodium dodecyl sulfate (SDS) polyacrylamide gels, followed by transfer onto nitrocellulose membranes (Bio-Rad, Hercules, CA). Membranes were blocked in 2.5% bovine serum albumin and incubated with the indicated primary antibodies overnight at 4 °C. The following primary antibodies were used: rabbit anti-ABCA1 (NB400-105, Novus); goat anti-apoE (AB947, Millipore, Burlington, MA); rabbit anti-LRP1 (ab92544, Abcam, Cambridge, UK); rabbit anti-c-Jun (9165, Cell Signaling, Danvers, MA); mouse anti-PHH3 (05-806, Millipore); rabbit anti-CD11b (ab133357, Abcam). Targeted proteins were detected by adding corresponding HRP-conjugated secondary antibody (Cell Signaling) and Clarity Western ECL Substrate (Bio-Rad). Membranes were digitally imaged using a GS-710 densitometer (Bio-Rad) and band densities were measured using NIH Image J software.

2.4. Cholesterol and triglyceride analyses in serum

Total serum cholesterol and triglycerides were quantified using

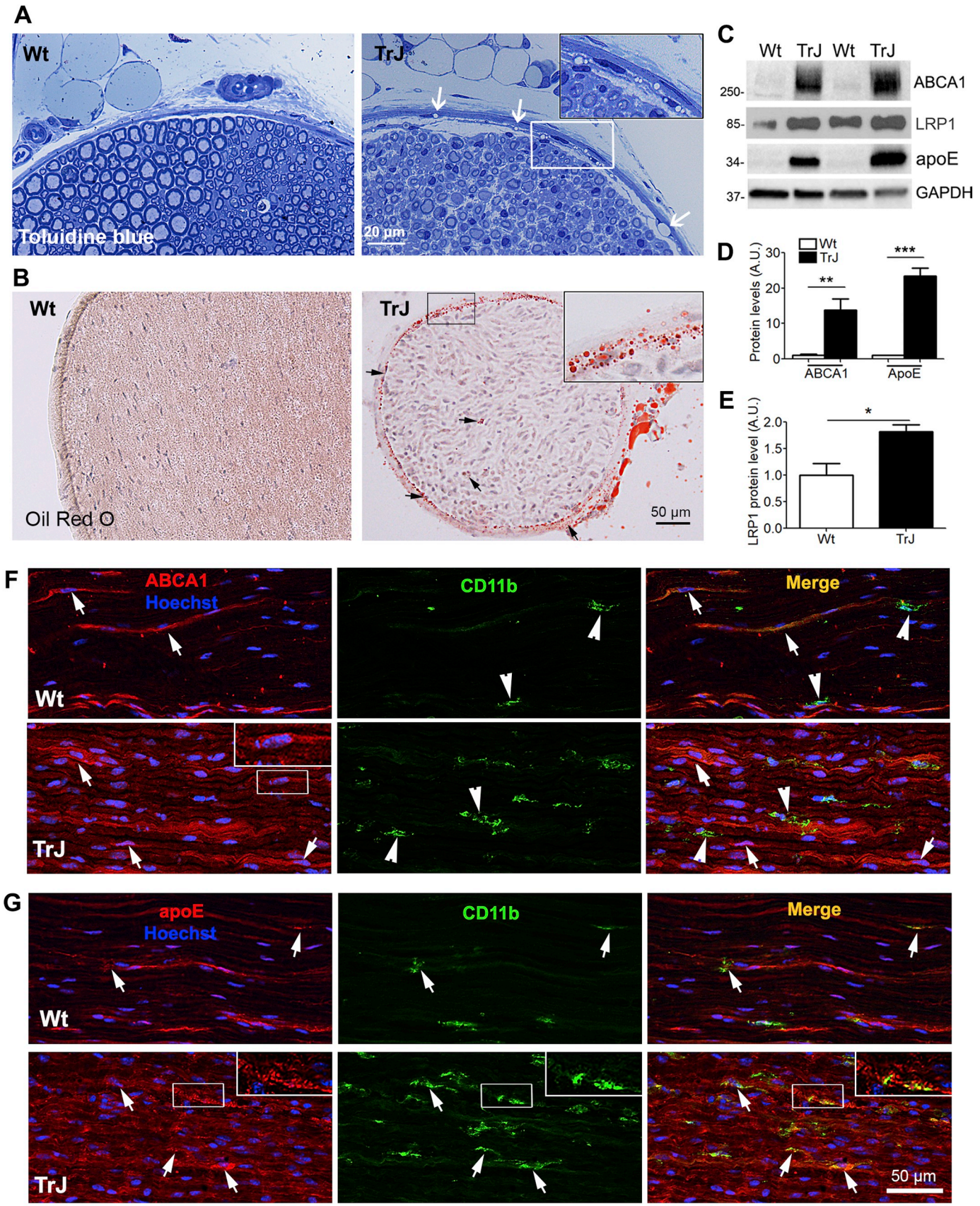

(caption on next page)

Fig.1. Lipid accumulation and elevated lipid metabolism related protein expression in sciatic nerves from 6-mo-old neuropathic mice.
(A) Toluidine blue staining reveals clear lipid droplets in the perineurium of neuropathic samples (arrows). (B) Oil Red O staining on sciatic nerve sections shows lipid droplets (arrows) in the perineurium and the endoneurium of the TrJ sample. Nuclei are in purple. (A, B) The marked areas are magnified in the upper right corners. (C) Representative immunoblots, and (D, E) quantification of ABCA1, apoE and LRP1 in sciatic nerves from 6-mo-old Wt and TrJ mice. GAPDH or Actin is shown as the loading control. A.U.: arbitrary unit; $n = 4$ nerves, per condition. Values represent the mean + SEM. $^{*}p < .05$, $^{**}p < .01$, $^{***}p < .001$, unpaired two-tailed Student's *t*-test. (F) Immunostaining for ABCA1 (red) with CD11b (green) in Wt and TrJ nerves shows ABCA1 in Schwann cells (arrows), rather than in macrophages (arrowheads). A magnified image of a Schwan cell is shown in the upper right corner of the TrJ nerve. (G) Colabeling of the nerves with anti-apoE and CD11b antibodies identifies macrophages as a cellular source for ApoE (arrows). Magnification, as shown. (For interpretation of the references to colour in this figure legend, the reader is referred to the web version of this article.)

Pointe Scientific Liquid Reagents (Thermo Fisher Scientific). Individual mouse serum samples were run in duplicate in a 96-well plate and measured for absorbance following manufacturer's protocol. For cholesterol profile analysis, we used 500 µL pools with equal volume contribution from individual mice within each group. Each pool was injected onto a Superose 6 Increase 10/300 GL size-exclusion column (GE Healthcare) and run at 0.5 mL/min in an aqueous mobile phase consisting of 0.15 M NaCl, 0.01 M Na_2PO_4, and 0.001 M EDTA. Fractions were collected every minute. Fractions (100 µL) were measured using Pointe Scientific reagents, as above, and µg/fraction was calculated.

2.5. Nerve morphological studies

Sciatic nerves were fixed in 2.5% glutaraldehyde in 0.1 M sodium cacodylate buffer, pH: 7.4 for 24 h at 4 °C. Subsequently, the samples were transferred to 0.1 M sodium cacodylate buffer (pH: 7.4) and processed for plastic embedding and Toluidine blue staining by the Emory University EM facility (Amici et al., 2006). Images were digitally captured using an Olympus BX43 upright microscope outfitted with an Olympus DP80 camera. For the morphometric studies, samples from 4 mice per group were analyzed by NIH Image J software. Within randomly selected, fixed nerve tissue areas, the cross-sectional area of each axon and nerve fiber were automatically or manually selected and measured, and the area size was converted to diameter using an equation: $2 \times \sqrt{area/\pi}$. G ratios were calculated as values of axon diameter/fiber diameter. The percentage of myelinated fibers within a fixed area was calculated by dividing the total number of axons with g-ratios < 1, by the total number of axons.

2.6. Immunohistochemical staining and fluorescence microscopy

Freshly-frozen sciatic nerves were sectioned at 8 µm thickness and fixed in 4% paraformaldehyde for 15 min. For Ki67, CD11b or apoE & CD11b co-staining, slides were permeabilized in ice-cold acetone for 2 min. For ABCA1 & CD11b co-staining, slides were permeabilized 0.2% Triton X-100 for 30 min. Sections were rinsed in PBS and blocked with 15% normal goat serum in PBS for 1 h. Subsequently, nerve sections were probed with primary antibodies overnight at 4 °C. The antibodies, rabbit anti-Ki67 (RPCA-Ki67, EnCor, Gainesville, FL), rat anti-CD11b (MA5-16528, Thermo Fisher), rabbit anti-apoE (ab20874, Abcam) or rabbit anti-ABCA1 (NB400-105, Novus) were diluted in 10% normal goat serum containing PBS. After washing in PBS, samples were incubated with appropriate fluorescent-dye conjugated secondary antibodies (Invitrogen, Carlsbad, CA) and Hoechst dye (1:1000, Invitrogen) to label nuclei. Slides were mounted using Prolong Anti-Fade Gold (Invitrogen). Images from four random areas of each nerve were captured using a Nikon Eclipse E800 microscopy system. Ki67 + and CD11b + cells were counted from captured images, and the nerve tissue area was calculated by the Nikon software. The sum of immunoreactive cells per 1 mm^2 nerve tissue area was graphed and analyzed.

2.7. Statistical analyses

Raw data were exported to GraphPad Prism to calculate mean ± standard error mean (S.E.M). Statistical significance was determined by performing unpaired two-tailed Student's *t*-tests or unpaired two-tailed Kolmogorov–Smirnov tests using GraphPad PRISM 8. Statistical significance was defined as $p < .05$.

3. Results

3.1. Pronounced dyslipidemia in nerves from TrJ mice with advanced neuropathy

To investigate the potential involvement of dyslipidemia in neuropathic nerve pathology, we examined samples from 6-month-old Wt and TrJ mice (Fig. 1). Morphological analyses of Toluidine blue stained cross sections revealed the presence of vacuoles around the perineurium in affected samples (Fig. 1A, arrows), but not in Wt. To complement these observations, we used Oil Red O, a fat-soluble diazol dye that labels neutral lipids, including cholesteryl esters, in red (Mehlem et al., 2013). Compared to age-matched Wt, we observed neutral lipid droplets in the endoneurium and especially in the perineurium of TrJ nerves (Fig. 1B, arrows), while the overall lipid-like red staining was decreased (Fig. 1B).

Next, we performed western blots on whole nerve lysates with antibodies against key lipid transport proteins, including ATP-binding cassette transporter (ABCA1) and apolipoprotein E (apoE) (Vance and Hayashi, 2010; Zhou et al., 2019) (Fig. 1C). As shown on the representative blot and by quantification, we identified a pronounced ~13-fold increase in ABCA1, while the levels of apoE were over 20-fold higher in TrJ, compared with Wt (Fig. 1C, D). Similarly, the low-density lipoprotein receptor-related protein-1 (LRP1), a member of the low-density lipoprotein (LDL) receptor gene family, was also upregulated by ~1.8-fold (Fig. 1C, E). An increase in glial expression of LRP has been observed in the injured peripheral nerve (Campana et al., 2006), and both apoE and ABCA1 are overproduced in nerves from PMP22-deficient neuropathic mice (Zhou et al., 2019).

Next we asked which cell types contribute to the elevated ABCA1 and apoE by co-staining nerve samples with ABCA1, or apoE, and CD11b, a macrophage marker (Fig. 1F, G). In agreement with the biochemical data (Fig. 1C) and our previous publication (Zhou et al., 2019), the level of ABCA1 in normal nerves is low, and is associated with thin endoneurial fibroblasts and Schwann cells (Fig. 1F, arrows). In samples from TrJ mice, enhanced ABCA1-like immunoreactivity is detected in Schwann cells (Fig. 1F, lower panel, arrows), which can be recognized by their oval nuclei (Notterpek et al., 1997). In comparison, macrophages were not immunoreactive for ABCA1, neither in WT nor in TrJ nerves (Fig. 1F, arrowheads). While ABCA1 has not been studied extensively in the PNS, apoE is known to be expressed by macrophages under nerve injury condition (Ignatius et al., 1986). Indeed, co-staining with anti-apoE and CD11b antibodies identified macrophages (Fig. 1G, arrows), along with Schwann cells and endoneurial fibroblasts displaying enhanced apoE-like reactivity in the TrJ nerves. Together, these findings indicate pronounced dyslipidemia in nerves from symptomatic 6-mo-old TrJ mice, with Schwann cells and macrophages markedly reacting to the myelin defects.

3.2. Elevated plasma cholesterol levels in Wt and TrJ mice after 6 weeks HFD intervention

Given the observed lipid abnormalities in nerves from 6-mo-old TrJ mice, we investigated the impact of a lipid-enriched diet on neuropathy

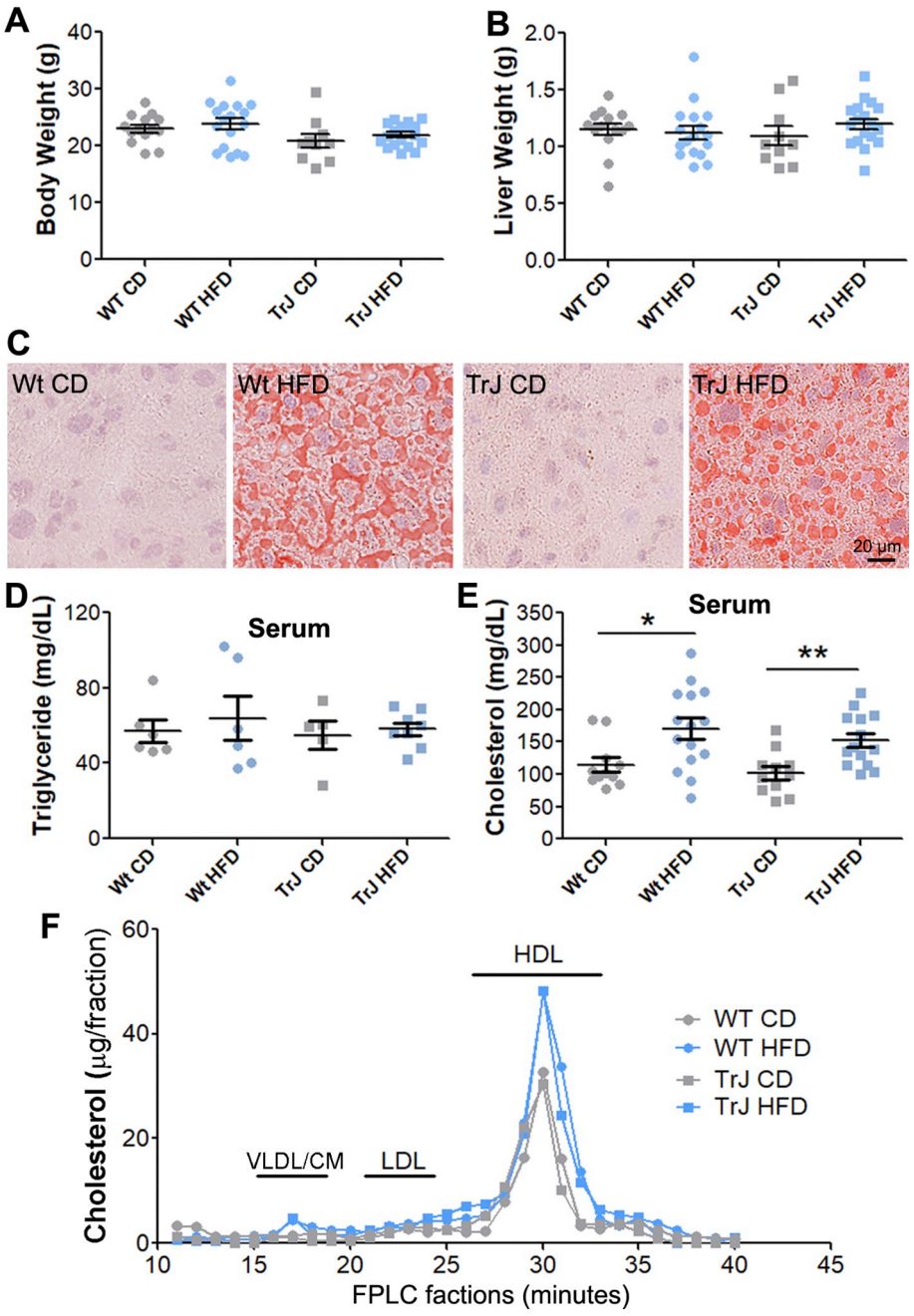

Fig. 2. Elevated cholesterol in the serum of Wt and TrJ mice after a 6-week-long HFD intervention.
(A) Body weight, and (B) liver weight of 9-week-old Wt and TrJ mice after feeding 6 weeks with control diet (CD) or HFD. n = 10–18 samples each group. (C) Oil red O staining on liver sections reveals lipid (red) accumulation in HFD groups. (D) Triglyceride, (E) total cholesterol levels, and (F) serum cholesterol distribution in different lipoprotein particles of Wt and TrJ mice with or without HFD. n = 5–16 samples each group. Values represent the mean ± SEM. *p < .05, **p < .01, unpaired two-tailed Student's t-test. VLDL/CM: Very-Low Density Lipoprotein/chylomicron remnant; LDL: Low Density Lipoprotein; HDL: High Density Lipoprotein. (For interpretation of the references to colour in this figure legend, the reader is referred to the web version of this article.)

development by randomly assigning 3-week-old male and female Wt and TrJ mice to a 6-week-long HFD intervention. Littermates from the same cohorts were given normal control diet (CD). The composition of each diet is shown in Table 1. At 9 weeks of age, the mice were collected and body weight, liver weight and serum triglycerides and cholesterol levels were measured (Fig. 2). The 6-week-long HFD intervention did not produce significant differences in body weight or liver weight, as compared with CD-fed mice (Fig. 2A, B). However, by Oil Red O staining the livers of both Wt and TrJ mice displayed obvious lipid accumulation in response to the HFD intervention (Fig. 2C). The six-week-long HFD feeding did not affect fasting triglyceride levels (Fig. 2D), while serum cholesterol levels were increased by ~50% in both Wt and TrJ mice (Fig. 2E). Fast protein liquid chromatography revealed that the majority of increased cholesterol was assembled in HDL particles (Fig. 2F). Overall, young Wt and TrJ neuropathic mice responded similarly to the 6-week-long HFD, without adverse effects.

3.3. Improved myelination in the sciatic and phrenic nerves of HFD-fed TrJ mice

To examine the impact of the HFD intervention on the pathogenesis of the neuropathy, we performed morphometric studies on sciatic and phrenic nerve cross sections (Figs. 3 and 4). In samples from Wt mice, the HFD diet did not cause detectable changes in the percentage of myelinated axons, fiber diameters or g-ratios (Fig. 3A–D). In comparison, nerves from HFD-fed TrJ mice demonstrated a notable increase in myelinated axons, which was significant upon quantification of individual fibers within randomly-chosen fixed tissue areas (64 ± 1% in TrJ CD vs. 86 ± 1% in TrJ HFD, p < .001) (Fig. 3A–B). In addition, the average fiber diameter increased (3.4 ± 0.1 μm in TrJ CD vs. 3.9 ± 0.1 μm in TrJ HFD, p < .01). Together these changes in axonal and fiber diameter resulted in lower g-ratios (axon diameter / fiber diameter) (0.83 ± 0.01 in TrJ CD vs. 0.76 ± 0.01 in TrJ HFD, p < .01), which is indicative of improvements in the maintenance of

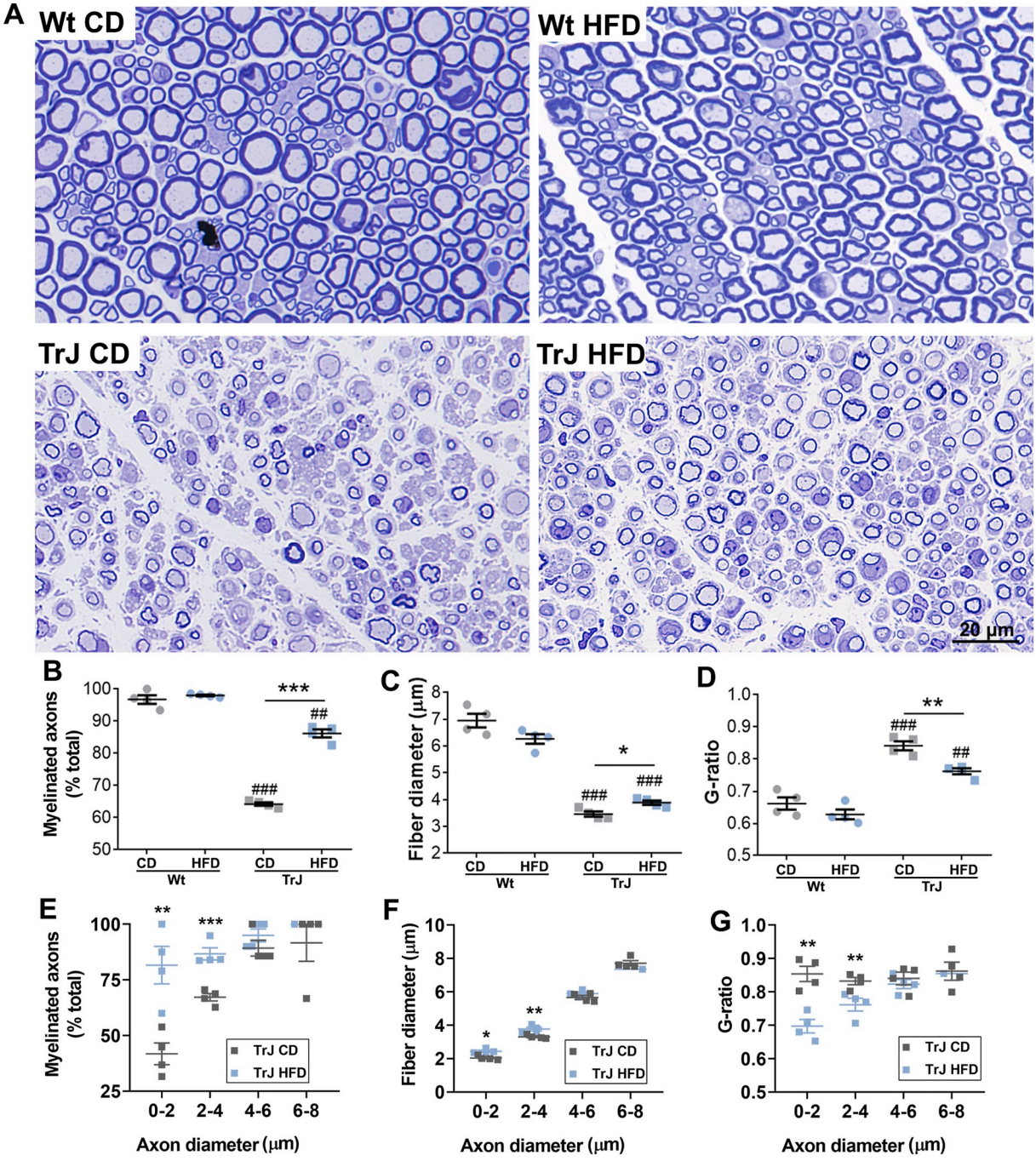

Fig. 3. Improved myelination in the sciatic nerve of TrJ mice after HFD intervention.
(A) Representative cross-sectional views of Toluidine blue stained sciatic nerve sections from Wt and TrJ mice, from the CD or HFD groups. (B, G) Morphometric analyses of the percentage of myelinated axons (B), fiber diameter (C) and g-ratio (D) on sciatic nerves from Wt and TrJ mice with or without HFD. Data were quantified from 70 to 100 fibers per nerve sample from 4 mice each group. The (E) percentage of myelinated fibers, (F) fiber diameter, and (G) g-ratios from TrJ sciatic nerves are graphed, after segregation of the data into 4 groups by fiber caliber. Values represent the mean ± SEM. $^{\#\#}p < .01$, $^{\#\#\#}p < .001$, compared to Wt CD; $^{*}p < .05$, $^{**}p < .01$, $^{***}p < .001$, unpaired two-tailed Student's t-test. ## identifies genotype effect. (For interpretation of the references to colour in this figure legend, the reader is referred to the web version of this article.)

myelinated fibers (Fig. 3A, C, D). To determine which fibers (small or large) responded to the HFD intervention, we analyzed the data from TrJ mice after segregating the axons by diameter into 4 groups (Fig. 3E–G). These detailed analyses revealed preferential response of small caliber myelinated fibers to the HFD intervention, and this was evident by the percentage of myelinated axons, fiber diameter, as well as in g-ratios (Fig. 3E–G).

To further examine the impact of the HFD on myelination, we also analyzed the phrenic nerves, which mostly contain myelinated motor fibers (Fig. 4). By morphological examination, nerves from HFD-fed TrJ mice display an increase in myelinated axonal profiles, which upon quantification is significant (Fig. 4A, B). Measurements of axon and fiber diameters, and calculation of g-ratios failed to detect changes in nerves from Wt mice, which agree with the representative micrographs (Fig. 4A–E). In samples from HFD-fed TrJ group, axon (Fig. 4C) and fiber (Fig. 4D) diameters were similar to those of CD-fed TrJ mice ($p = .6707$ and $p = .2050$, respectively), however these measurements yielded a significant improvement in g-ratios (Fig. 4E). Therefore, the

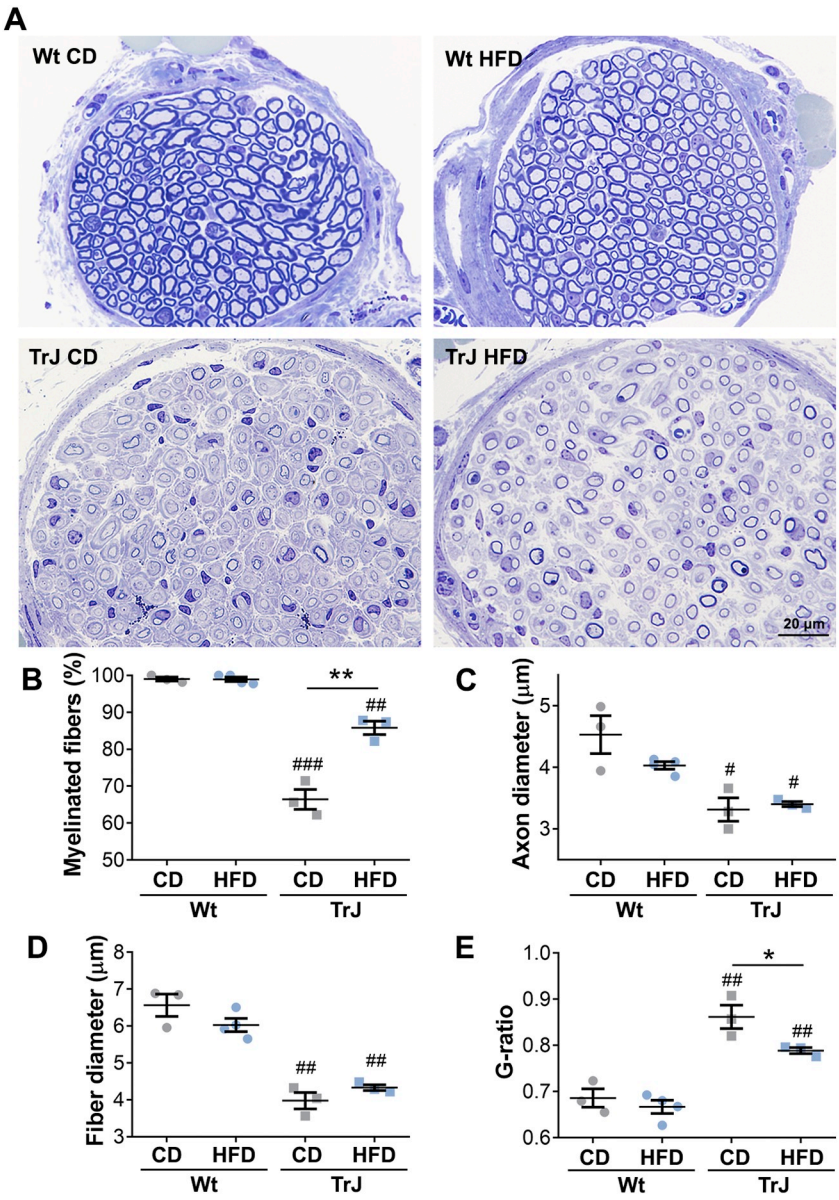

Fig. 4. Improved myelination in the phrenic nerve of TrJ mice after 6-week HFD intervention.
(A) Representative cross-sectional views of Toluidine blue stained phrenic nerve sections from Wt and TrJ mice, from the CD or HFD groups. (B-E) Morphometric analyses of the percentage of myelinated axons (B), axon diameter (C), fiber diameter (D), and g-ratio (E) in phrenic nerves from Wt and TrJ mice, with or without HFD. Data were quantified from 70 to 100 fibers per nerve sample from 3 to 4 mice each group. Values represent the mean ± SEM. $^{\#}p < .05$, $^{\#\#}p < .01$, $^{\#\#\#}p < .001$, compared to Wt CD; $^{*}p < .05$, $^{**}p < .01$, $^{***}p < .001$, unpaired two-tailed Student's t-test. (For interpretation of the references to colour in this figure legend, the reader is referred to the web version of this article.)

neutral lipid-enriched HFD benefitted small caliber myelinated axons in the sciatic (Fig. 3), as well as motor axons in the phrenic nerve (Fig. 4).

3.4. Cellular proliferation is reduced in the sciatic nerves of HFD-fed TrJ mice

Aberrant Schwann cell proliferation is a common feature of PMP22-linked neuropathies, including early-onset conditions (Notterpek and Tolwani, 1999). Therefore, we assessed cellular markers related to Schwann cell differentiation and mitosis in nerves from the four study groups (Fig. 5). Elevated expression of c-Jun, a negative regulator of myelination, has been described in denervated but not myelinating Schwann cells (Shy et al., 1996; Jessen and Mirsky, 2008). Indeed, the levels of c-Jun and the mitotic marker phosphohistone H3 (PHH3) were significantly elevated in CD-fed TrJ nerves, compared with Wt (Fig. 5A–D). Significantly, in response to the HFD intervention, the expression of both of these molecules decreased (Fig. 5A–D), a finding that agrees with the observed improvements in myelination (Figs. 3, 4). The aberrant mitotic phenotype of neuropathic nerves was also evident through immunostaining and counting the number of Ki67-positive cells (Scholzen and Gerdes, 2000; Lee et al., 2018) in nerves from CD-fed Wt and TrJ mice, which identified a strong genotype effect (Fig. 5E–H). Significantly, we discovered a ~2.3-fold decrease in the number of Ki67-positive cells after the HFD intervention (Fig. 5E, F), a result that is supported by counting total cell numbers within fixed nerve tissue areas (Fig. 5G, H). Together these results indicate that the HFD intervention supported the maintenance of the myelinated Schwann cell phenotype in nerves from young neuropathic mice.

3.5. Macrophage infiltration is reduced in nerves from HFD-fed neuropathic mice

Macrophage infiltration is known to occur in nerve injury and in hereditary neuropathies, as Schwann cells attract immune cells to aid in the clearance of myelin debris (Martini et al., 2008). Nerves of 9-week-old CD-fed Wt and TrJ mice contain over one hundred, or over three hundred, CD11b-positive macrophages per square mm, respectively (Fig. 6A, B). After 6 weeks on the HFD intervention, macrophage numbers were reduced in both genotypes, with neuropathic nerves mimicking the cell counts from Wt (Fig. 6A, B). Western blot analyses of total nerve lysates from the CD-fed cohort supported the morphological observations, with elevated CD11b TrJ samples, compared with Wt

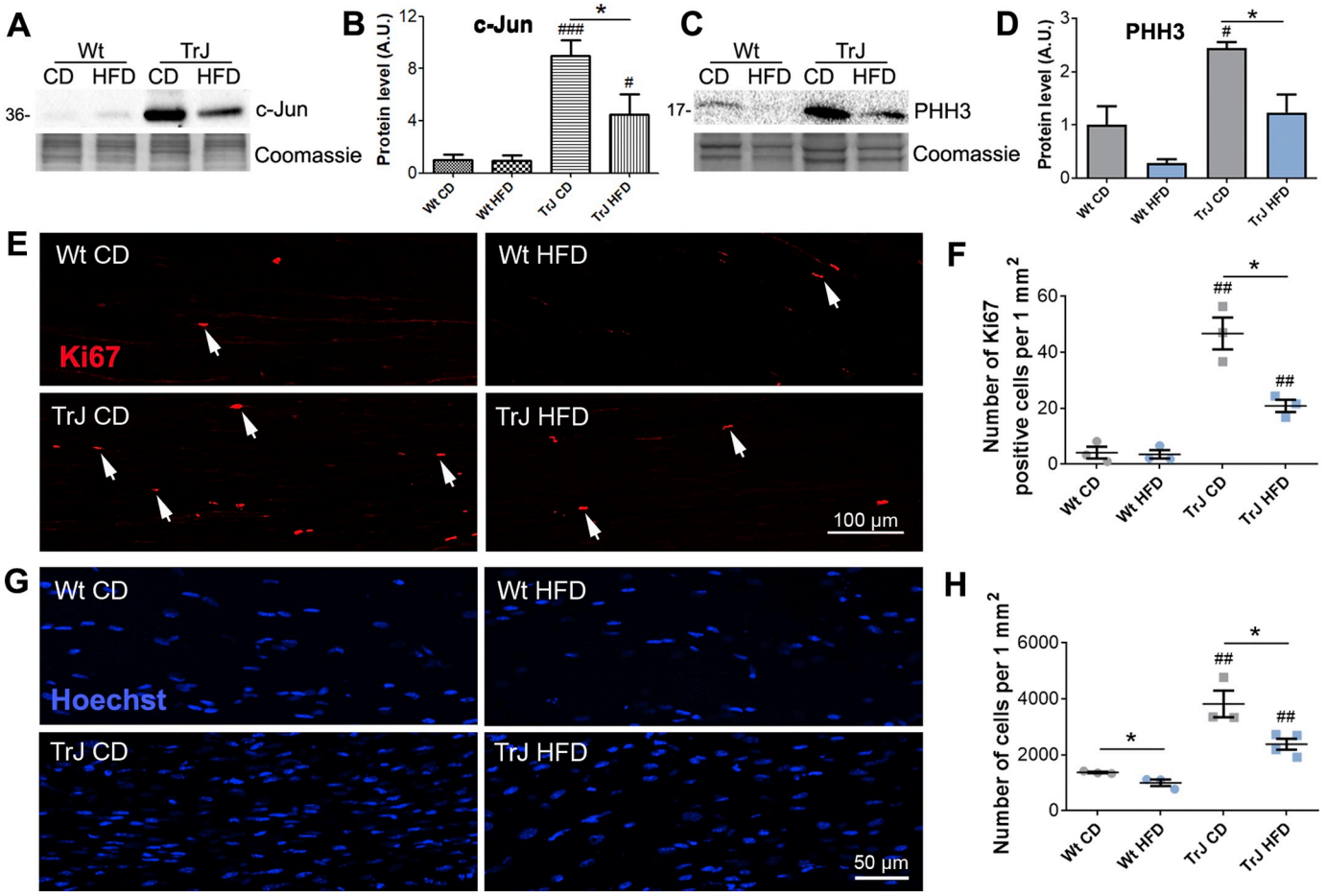

Fig. 5. Reduction in cellular proliferation in neuropathic nerves after HFD.
Representative immunoblots and quantification of c-Jun (A–B) and PHH3 (C–D) in sciatic nerve lysates from Wt and TrJ mice after CD or HFD intervention. (E) Representative images and (F) quantification of Ki67-positive cells in sciatic nerves of Wt and TrJ mice with CD or HFD. (G) Representative images and (H) quantification of Hoechst nuclear stain in sciatic nerves of Wt and TrJ mice after CD or HFD. Images from Coomassie stained gels are shown as the protein loading control. A.U.: arbitrary unit; Values represent the mean ± SEM. $^{\#}p < .05$, $^{\#\#}p < .01$, $^{\#\#\#}p < .001$, compared to Wt CD; $^{*}p < .05$; unpaired two-tailed Student's *t*-test. n = 3–6 nerves per each group. # identifies genotype effect.

(Fig. 6C, D). However, CD11b protein levels were diminished after the HFD intervention, as suggested by the reduction in macrophage numbers. Finally, the elevated endogenous nerve IgG levels in TrJ samples were also partially rectified by the HFD diet, likely due to decreased permeability of the blood-nerve and/or perineurial barriers. Together, these results suggest attenuated immune activation by the fat-enriched diet (Fig. 6E, F).

3.6. Partial correction of nerve dyslipidemia by HFD intervention

Given the pronounced dyslipidemia in advanced neuropathic nerves (Fig. 1), we asked whether the HFD intervention altered this phenotype (Figs. 7 and 8). As shown on the Oil Red O stained micrographs, at 9 weeks of age, nerves from TrJ mice already contain an abundance of neutral lipids at the perineurium, compared with Wt (Fig. 7A). In response to HFD, we did not observe a significant change in the density of lipid droplets at the perineurium in either genotype, while an increase in neutral lipid clusters was observed within the endoneurium of HFD-fed TrJ mice (Fig. 7A–C). Upon quantification, nerves from TrJ HFD mice displayed similar density of perineurial lipid droplets as the CD-fed group (Fig. 7B), while endoneurial lipid droplets increased ~3-fold (2.1 ± 0.1 in TrJ CD vs. 6.2 ± 0.6 in TrJ HFD) (Fig. 7C). Lipid droplets were absent from nerves of Wt mice regardless of diet (Fig. 7A, top).

To complement the morphological lipid localization studies (Fig. 7A–C), we examined the influence of HFD on biochemical markers of dyslipidemia (Fig. 8). At 9 weeks of age, in TrJ neuropathic nerves, the expression of ABCA1, apoE, and LRP1 were already significantly elevated when compared with age-matched CD-fed Wt (Fig. 8A–F). The HFD intervention moderated this atypical phenotype concerning apoE and LRP1, however, ABCA1 levels were not reduced significantly compared with CD-fed TrJ (Fig. 8A–F). Together, these results demonstrate the strong influence of a short-term diet intervention on lipid metabolism in neuropathic nerves.

4. Discussion

Here, we show that developing TrJ neuropathic nerves actively respond to dietary lipids, with improved myelination and alleviated nerve pathologies. Our data revealed the beneficial impact of a neutral lipid-enriched diet on ameliorating the extent of pathogenesis of the neuropathy during post-weaning period, as indicated by morphological and biochemical measures. Compared with CD-fed TrJ mice, the degree of dyslipidemia was also attenuated by the HFD intervention, as detected by changes in the levels of cholesterol transport proteins. Together, our findings reveal a pronounced influence of dietary lipids on neuropathic nerves and support further work toward understanding the involvement of lipid metabolism in myelin disorders.

How did the neutral-lipid enriched HFD improve myelination in young TrJ mice? While the current study did not investigate the

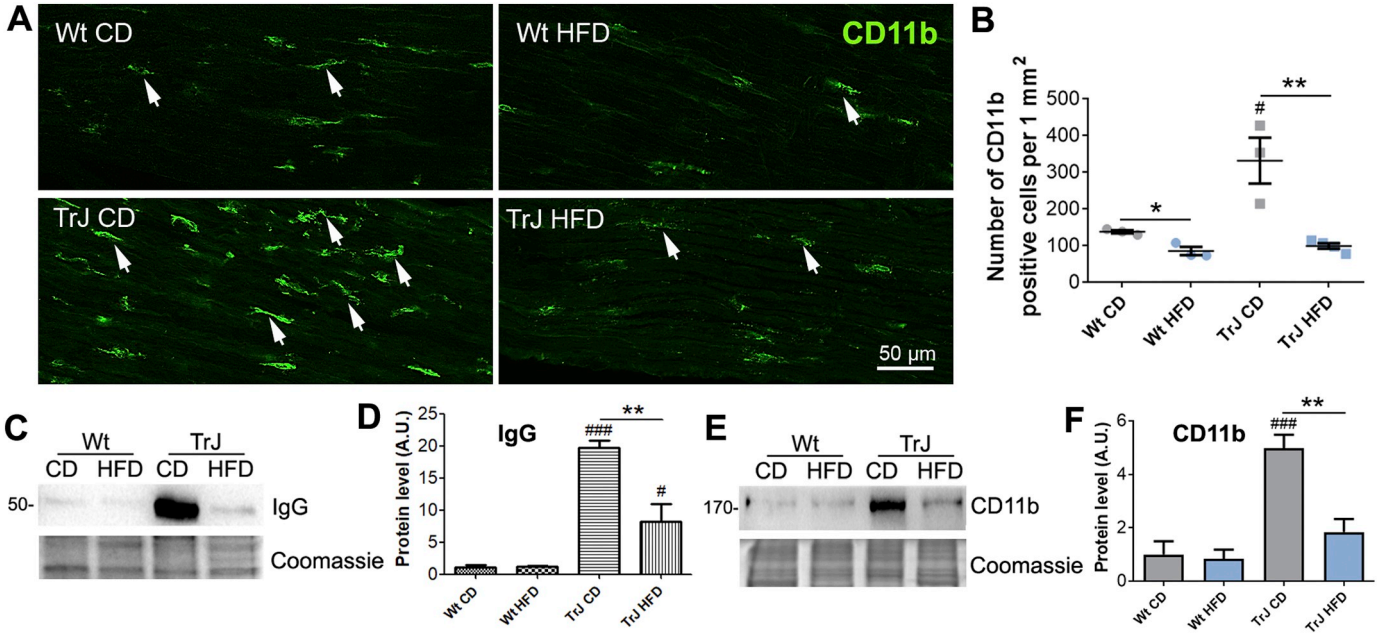

Fig. 6. Fewer macrophages in neuropathic nerves in response to HFD.
(A) Representative images, and (B) quantification of CD11b-positive immune cells in the indicated nerves. Representative immunoblots and quantification of CD11b (C–D) and IgG (*E*–F) in lysates from sciatic nerves of Wt and TrJ mice after CD or HFD. Coomassie stained gel images are shown as the loading control. A.U.: arbitrary unit; Values represent the mean ± SEM. $^{\#}p < .05$, $^{\#\#\#}p < .001$, compared to Wt CD; $^{**}p < .01$; unpaired two-tailed Student's *t*-test. n = 3–6 each group. # identifies genotype effect.

mechanism of uptake for the dietary lipids by the nerves, previous studies in both CNS and PNS demonstrated the importance of cholesterol in myelin development and regeneration (Saher et al., 2005; Saher et al., 2009). In the CNS, cholesterol esters are partially localized to newly-formed myelin and a cholesterol ester hydrolase, necessary for free cholesterol conversion, is specifically found in myelin (Adams and Davison, 1959; Eto and Suzuki, 1973). In degenerating/regenerating peripheral nerves, most lipid species are decreased, while cholesterol esters are dramatically increased (Larrouquere-Regnier et al., 1979; Yao and Dyck, 1981; Hofteig et al., 1982) and stored as lipid droplets in Schwann cells and perineurial/endoneurial fibroblasts to facilitate myelin regeneration (Rawlins et al., 1972; White et al., 1989; Goodrum et al., 1994). In agreement, our data revealed the accumulation of neutral lipid clusters in the endoneurial and perineurial area of

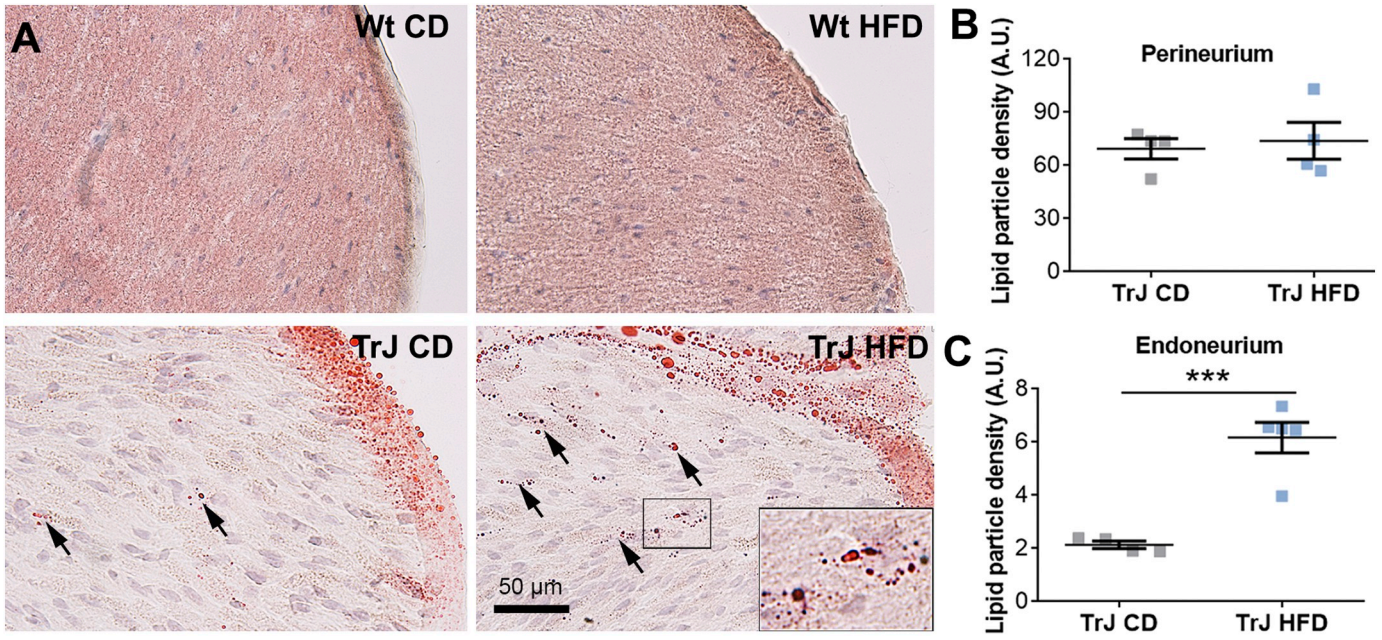

Fig. 7. Increase in endoneurial lipid droplets in neuropathic nerves after HFD intervention.
(A) Oil Red O staining on cross-sectioned sciatic nerves from 9-week-old Wt and TrJ mice after CD or HFD. Nuclei are in purple. Arrows mark endoneurial lipid droplets in neuropathic nerves. (B, C) Quantification of lipid particle density in the perineurium and the endoneurium, as detected by Oil Red O. Values represent the mean ± SEM. $^{***}p < .001$, unpaired two-tailed Student's *t*-test. A.U.: arbitrary unit; n = 4–5 nerves per each group. (For interpretation of the references to colour in this figure legend, the reader is referred to the web version of this article.)

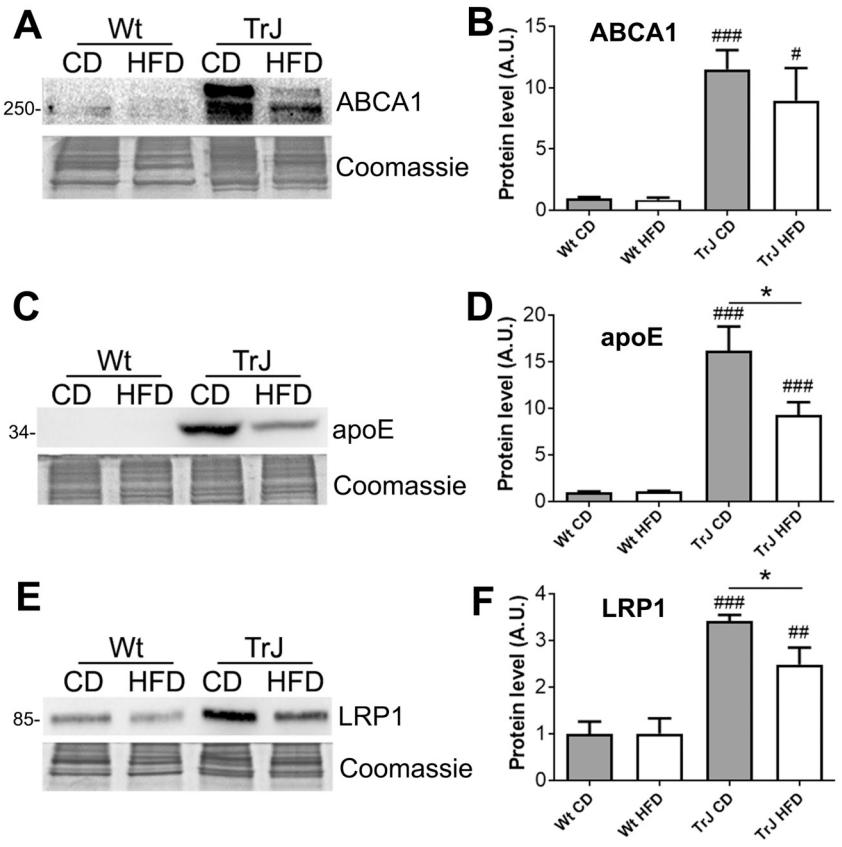

Fig. 8. Attenuated dyslipidemia in neuropathic nerves after HFD intervention.

(A–F) Representative immunoblots and quantification of ABCA1 (A, B), apoE (C, D) and LRP1 (E, F) in sciatic nerves from Wt and TrJ mice after CD or HFD. Images from Coomassie stained gels are shown as the loading control. A.U.: arbitrary unit; Values represent the mean + SEM. $^{\#}p < .05$, $^{\#\#}p < .01$, $^{\#\#\#}p < .001$, compared to Wt CD; $^{*}p < .05$, unpaired two-tailed Student's *t*-test. n = 5–6 each group. # identifies genotype effect.

neuropathic nerves from 6-month- and 9-week-old CD-fed TrJ mice, with an increase in endoneurial lipid deposits with HFD feeding. The presence of lipid droplets within the endoneurium of HFD-fed TrJ mice may reflect the uptake of exogenous lipids by nerve fibroblasts and Schwann cells. The molecular and cellular mechanisms of lipid uptake will be important to study in the future and will need to include various disease stages. It is possible that Schwann cells within nerves of young neuropathic animals respond preferentially to the HFD intervention and able to partially rescue the dysmyelinating phenotype.

The neutral lipid-enriched HFD not only improved nerve myelination, but also supported a myelination-permissive environment, as indicated by a reduction in aberrant cell proliferation and in c-Jun expression. In response to nerve injury, myelinated Schwann cells undergo de-differentiation in an attempt to remyelinate regenerating axons (Jessen et al., 2015). In our study, the reduction in mitotic cells in HFD-fed young neuropathic mice is likely the reflection of enhanced differentiation. Indeed, TrJ nerves are delayed in development, with a pronounced dysmyelinating phenotype by 10 days of postnatal development (Notterpek et al., 1997). The HFD intervention also reduced CD11b-positive macrophage infiltration, a sign of myelin damage in injured and neuropathic nerves (Martini et al., 2008). Along with the reduction in cellular proliferation and macrophage infiltration, HFD supported the maintenance of axons and myelin thickness, as indicated by the results from the morphometric studies. Similar improvements in myelination and rescue of myelinated axons were achieved in CMT1A neuropathic rats by a phosphatidylcholine-enriched diet (Fledrich et al., 2018).

With regard to systemic lipid metabolism, the 6-week-long HFD regimen increased circulatory serum cholesterol levels in both Wt and TrJ, but only affected nerve morphology in neuropathic mice. For example, endoneurial lipid deposits after HFD were observed only in the neuropathic nerves (Fig. 7), suggesting an active entry of circulatory lipids into the neural tissue. The source of the elevated neutral lipids was likely from the epineurial adipocytes, in part, reacting as a compensatory mechanism (Verheijen et al., 2003; Montani et al., 2018). Our findings in nerves of Wt mice agree with published reports on de novo lipid synthesis within neural tissues and the lack of lipid uptake from the plasma (Jurevics and Morell, 1994; Verheijen et al., 2003; Schmitt et al., 2015). However, in TrJ nerves, the circulation could be partially responsible for the lipid deposits, as the blood-nerve barrier might be more permeable under neuropathic condition (Bouldin et al., 1991; Kanda, 2013).

While the direct mechanism by which HFD intervention benefits myelination remains to be determined, it is important to note that PMP22 contains evolutionarily conserved cholesterol binding CARC and CRAC domains (Gould et al., 2005; Sedzik et al., 2013) and is known to regulate Schwann cell differentiation both in vivo and in vitro (Magyar et al., 1996; Hanemann et al., 1997; Nobbio et al., 2004). Interestingly, among ~40 different PMP22 missense mutations, 4 were localized to the CARC and 7 were found in the CRAC domain, with CRAC-mutant patients displaying severe, early-onset neuropathic phenotypes (Navon et al., 1996; Bort et al., 1997; Ionasescu et al., 1997; Ikegami et al., 1998; Marques Jr. et al., 1998; Parman et al., 1999; Numakura et al., 2000; Ohnishi et al., 2000). Hence, the added cholesterol (0.2% of total calories) in the HFD may improve myelination and alleviate Schwann cell over-proliferation by modulating PMP22 signaling. In addition, independent of PMP22, cholesterol is known to regulate the PI3K/AKT/mTOR pathway, which is involved in myelination (Norrmen et al., 2014; Domenech-Estevez et al., 2016; Mathews and Appel, 2016). The currently tested HFD, with 0.2% cholesterol, significantly increased serum cholesterol levels, which may have contributed to the positive outcome with regards to nerve pathology. Dietary cholesterol was recently shown to promote the repair of demyelinated lesions in the CNS by creating a permissive environment (Berghoff et al., 2017). Moreover, a cholesterol-enriched diet, with 5% cholesterol content, was used to treat mice with CNS demyelinating Pelizaeus-Merzbacher disease (Saher et al., 2012) caused by the overexpression of proteolipid protein (Werner et al., 2013). While

cholesterol-enriched diets have not been tested in early-onset hereditary neuropathic rodents, our previous in vitro studies suggest that cholesterol supplementation could provide benefits to affected nerves in certain genetic conditions. Specifically, in Schwann cells cultured from PMP22-deficient mice, exogenous cholesterol supplementation corrected aberrant cellular morphology and improved cell migratory behavior (Lee et al., 2014).

Dietary lipid supplementation and/or substitutions have been explored in numerous neurological conditions as potential therapies (Saher et al., 2005; Saher et al., 2012; Berghoff et al., 2017; Fledrich et al., 2018). The percentage of cholesterol and of specific lipids varies among the various HFD interventions, which may sometimes contribute to seemingly opposing results in the literature. For example, in C57BL/6 mice, which is the genetic background of the TrJ (Henry and Sidman, 1983), a 14-week-long HFD caused damage to large myelinated and small sensory nerve fibers, leading to neuropathy (Xu et al., 2014). In this long-term study, 45% of the calories were derived from lard fat and the percentage of cholesterol was 0.02% in comparison to 42% milk fat with 0.2% cholesterol in our study (Table 1). In addition to the specific diet, the length of the intervention as well as the strain and the age of mice have strong influence on the outcome. Here, as mentioned above, we treated young mice with developing nerve pathology, which may have been key for the observed improvements. Indeed, in a previous report, soluble neuregulin-1 significantly improved CMT1A nerve myelination when animals were treated before weaning age (P6-P18) (Fledrich et al., 2014). The neuregulin-1 therapy impacted myelin development, including Schwann cell differentiation, by enhancing the PI3K-AKT signaling (Fledrich et al., 2014). Coincidently, neuregulin-1 in Schwann cells increases the activity of 3-hydroxy-3-methylglutaryl-CoA (HMGCoA) reductase, a key enzyme in cholesterol biosynthesis (Pertusa et al., 2007). Therefore, the lipid pathway may have been responsible, in part, for the positive effects in the cited study.

Additional studies are necessary to determine the optimal lipid-enriched diet, treatment time window and length to achieve long-lasting benefits in neuropathic nerves without harmful side effects. Nerve conduction and muscle strength studies will need to be included for comprehensive evaluation. Alternatively, intermittent lipid supplementation throughout the lifespan of the organism may be ideal. In addition, considering the phenotype heterogeneity due to the variety of mutations in human PMP22 (Li et al., 2013), it will be informative to study the effects of lipid-enriched diets in multiple animal models, such as with PMP22 duplication, deletion and other missense mutations. Overall, our studies support recent findings on the positive influence of dietary lipids on myelination and myelin repair.

Declaration of Competing Interest

The authors declare no competing financial interests.

Acknowledgements

These studies were supported, in part, by funds from the Facial Pain Research Foundation and the UF College of Medicine to L.N. We thank Hong Yi at the Emory University Robert P. Apkarian Integrated Electron Microscopy Core for sample processing and Toluidine blue staining. Studies at OHSU were partially supported by NIH grant HL57986 to S.F and by AHA grant 16SDG27520011 to H.T.

References

Adams, C.W., Davison, A.N., 1959. The occurrence of esterified cholesterol in the developing nervous system. J. Neurochem. 4, 282–289.
Amici, S.A., Dunn Jr., W.A., Murphy, A.J., Adams, N.C., Gale, N.W., Valenzuela, D.M., Yancopoulos, G.D., Notterpek, L., 2006. Peripheral myelin protein 22 is in complex with alpha6beta4 integrin, and its absence alters the Schwann cell basal lamina. J. Neurosci. 26, 1179–1189.
Berghoff, S.A., Gerndt, N., Winchenbach, J., Stumpf, S.K., Hosang, L., Odoardi, F., Ruhwedel, T., Bohler, C., Barrette, B., Stassart, R., Liebetanz, D., Dibaj, P., Mobius, W., Edgar, J.M., Saher, G., 2017. Dietary cholesterol promotes repair of demyelinated lesions in the adult brain. Nat. Commun. 8, 14241.
Berry, J.F., Cevallos, W.H., Wade Jr., R.R., 1965. Lipid class and fatty acid composition of intact peripheral nerve and during Wallerian degeneration. J. Am. Oil Chem. Soc. 42, 492–500.
Bort, S., Nelis, E., Timmerman, V., Sevilla, T., Cruz-Martinez, A., Martinez, F., Millan, J.M., Arpa, J., Vilchez, J.J., Prieto, F., Van Broeckhoven, C., Palau, F., 1997. Mutational analysis of the MPZ, PMP22 and Cx32 genes in patients of Spanish ancestry with Charcot-Marie-Tooth disease and hereditary neuropathy with liability to pressure palsies. Hum. Genet. 99, 746–754.
Bouldin, T.W., Earnhardt, T.S., Goines, N.D., 1991. Restoration of blood-nerve barrier in neuropathy is associated with axonal regeneration and remyelination. J. Neuropathol. Exp. Neurol. 50, 719–728.
Brady, S.T., Siegel, G.J., Albers, R.W., Price, D.L., 2011. Basic neurochemistry: Principles of molecular, cellular, and medical neurobiology 8th edition: Elsevier Science.
Campana, W.M., Li, X., Dragojlovic, N., Janes, J., Gaultier, A., Gonias, S.L., 2006. The low-density lipoprotein receptor-related protein is a pro-survival receptor in Schwann cells: possible implications in peripheral nerve injury. J. Neurosci. 26, 11197–11207.
Cermenati, G., Audano, M., Giatti, S., Carozzi, V., Porretta-Serapiglia, C., Pettinato, E., Ferri, C., D'Antonio, M., De Fabiani, E., Crestani, M., Scurati, S., Saez, E., Azcoitia, I., Cavaletti, G., Garcia-Segura, L.M., Melcangi, R.C., Caruso, D., Mitro, N., 2015. Lack of sterol regulatory element binding factor-1c imposes glial fatty acid utilization leading to peripheral neuropathy. Cell Metab. 21, 571–583.
Clouet, P.M., Bourre, J.M., 1988. Ketone body utilization for lipid synthesis in the murine sciatic nerve: alterations in the dysmyelinating trembler mutant. J. Neurochem. 50, 1494–1497.
DiVincenzo, C., Elzinga, C.D., Medeiros, A.C., Karbassi, I., Jones, J.R., Evans, M.C., Braastad, C.D., Bishop, C.M., Jaremko, M., Wang, Z., Liaquat, K., Hoffman, C.A., York, M.D., Batish, S.D., Lupski, J.R., Higgins, J.J., 2014. The allelic spectrum of Charcot-Marie-Tooth disease in over 17,000 individuals with neuropathy. Mol. Genet. Genomic. Med. 2, 522–529.
Domenech-Estevez, E., Baloui, H., Meng, X., Zhang, Y., Deinhardt, K., Dupree, J.L., Einheber, S., Chrast, R., Salzer, J.L., 2016. Akt regulates axon wrapping and myelin sheath thickness in the PNS. J. Neurosci. 36, 4506–4521.
D'Urso, D., Prior, R., Greiner-Petter, R., Gabreels-Festen, A.A., Muller, H.W., 1998. Overloaded endoplasmic reticulum-Golgi compartments, a possible pathomechanism of peripheral neuropathies caused by mutations of the peripheral myelin protein PMP22. J. Neurosci. 18, 731–740.
Ekins, S., Litterman, N.K., Arnold, R.J., Burgess, R.W., Freundlich, J.S., Gray, S.J., Higgins, J.J., Langley, B., Willis, D.E., Notterpek, L., Pleasure, D., Sereda, M.W., Moore, A., 2015. A brief review of recent Charcot-Marie-Tooth research and priorities. F1000Res 4:53.
Eto, Y., Suzuki, K., 1973. Enzymes of cholesterol ester metabolism in the brain of mutant mice, quaking and jimpy. Exp. Neurol. 41, 222–226.
Feldman, E.L., Nave, K.A., Jensen, T.S., Bennett, D.L.H., 2017. New horizons in diabetic neuropathy: mechanisms, bioenergetics, and pain. Neuron 93, 1296–1313.
Fledrich, R., Schlotter-Weigel, B., Schnizer, T.J., Wichert, S.P., Stassart, R.M., Meyer zu Hörste, G., Klink, A., Weiss, B.G., Haag, U., Walter, M.C., Rautenstrauss, B., Paulus, W., Rossner, M.J., Sereda, M.W., 2012. A rat model of Charcot-Marie-Tooth disease 1A recapitulates disease variability and supplies biomarkers of axonal loss in patients. Brain 135, 72–87.
Fledrich, R., Stassart, R.M., Klink, A., Rasch, L.M., Prukop, T., Haag, L., Czesnik, D., Kungl, T., Abdelaal, T.A., Keric, N., Stadelmann, C., Bruck, W., Nave, K.A., Sereda, M.W., 2014. Soluble neuregulin-1 modulates disease pathogenesis in rodent models of Charcot-Marie-Tooth disease 1A. Nat. Med. 20, 1055–1061.
Fledrich, R., et al., 2018. Targeting myelin lipid metabolism as a potential therapeutic strategy in a model of CMT1A neuropathy. Nat. Commun. 9, 3025.
Fortun, J., Dunn Jr., W.A., Joy, S., Li, J., Notterpek, L., 2003. Emerging role for autophagy in the removal of aggresomes in Schwann cells. J. Neurosci. 23, 10672–10680.
Fridman, V., et al., 2015. CMT subtypes and disease burden in patients enrolled in the inherited neuropathies consortium natural history study: a cross-sectional analysis. J. Neurol. Neurosurg. Psychiatry 86, 873–878.
Goodrum, J.F., Earnhardt, T., Goines, N., Bouldin, T.W., 1994. Fate of myelin lipids during degeneration and regeneration of peripheral nerve: an autoradiographic study. J. Neurosci. 14, 357–367.
Gould, R.M., Morrison, H.G., Gilland, E., Campbell, R.K., 2005. Myelin tetraspan family proteins but no non-tetraspan family proteins are present in the ascidian (Ciona intestinalis) genome. Biol. Bull. 209, 49–66.
Hanemann, C.O., Gabreels-Festen, A.A., Stoll, G., Muller, H.W., 1997. Schwann cell differentiation in Charcot-Marie-Tooth disease type 1A (CMT1A): normal number of myelinating Schwann cells in young CMT1A patients and neural cell adhesion molecule expression in onion bulbs. Acta Neuropathol. 94, 310–315.
Henry, E.W., Sidman, R.L., 1983. The murine mutation trembler-J: proof of semidominant expression by use of the linked vestigial tail marker. J. Neurogenet. 1, 39–52.
Hofteig, J.H., Vo, P.N., Yates, A.J., Leon, K.S., 1982. Peripheral nerve phospholipid composition: development in normal nerve and age-dependent changes in Wallerian degenerated nerve. J. Neurochem. 39, 401–408.
Ignatius, M.J., Gebicke-Harter, P.J., Skene, J.H., Schilling, J.W., Weisgraber, K.H., Mahley, R.W., Shooter, E.M., 1986. Expression of apolipoprotein E during nerve degeneration and regeneration. Proc. Natl. Acad. Sci. U. S. A. 83, 1125–1129.
Ikegami, T., Ikeda, H., Aoyama, M., Matsuki, T., Imota, T., Fukuuchi, Y., Amano, T., Toyoshima, I., Ishihara, Y., Endoh, H., Hayasaka, K., 1998. Novel mutations of the peripheral myelin protein 22 gene in two pedigrees with Dejerine-Sottas disease. Hum. Genet. 102, 294–298.
Ionasescu, V.V., Searby, C.C., Ionasescu, R., Chatkupt, S., Patel, N., Koenigsberger, R.,

1997. Dejerine-Sottas neuropathy in mother and son with same point mutation of PMP22 gene. Muscle Nerve 20, 97–99.
Jackman, N., Ishii, A., Bansal, R., 2009. Oligodendrocyte development and myelin biogenesis: parsing out the roles of glycosphingolipids. Physiology (Bethesda) 24, 290–297.
Jessen, K.R., Mirsky, R., 2008. Negative regulation of myelination: relevance for development, injury, and demyelinating disease. Glia 56, 1552–1565.
Jessen, K.R., Mirsky, R., Lloyd, A.C., 2015. Schwann cells: development and role in nerve repair. Cold Spring Harb. Perspect. Biol. 7, a020487.
Juguelin, H., Heape, A., Boiron, F., Cassagne, C., 1986. A quantitative developmental study of neutral lipids during myelinogenesis in the peripheral nervous system of normal and trembler mice. Brain Res. 390, 249–252.
Jurevics, H.A., Morell, P., 1994. Sources of cholesterol for kidney and nerve during development. J. Lipid Res. 35, 112–120.
Kanda, T., 2013. Biology of the blood-nerve barrier and its alteration in immune mediated neuropathies. J. Neurol. Neurosurg. Psychiatry 84, 208–212.
Larrouquere-Regnier, S., Boiron, F., Darriet, D., Cassagne, C., Bourre, J.M., 1979. Lipid composition of sciatic nerve from dysmyelinating trembler mouse. Neurosci. Lett. 15, 135–139.
Lee, S., Amici, S., Tavori, H., Zeng, W.M., Freeland, S., Fazio, S., Notterpek, L., 2014. PMP22 is critical for actin-mediated cellular functions and for establishing lipid rafts. J. Neurosci. 34, 16140–16152.
Lee, S., Bazick, H., Chittoor-Vinod, V., Al Salihi, M.O., Xia, G., Notterpek, L., 2018. Elevated peripheral myelin protein 22, reduced mitotic potential, and proteasome impairment in dermal fibroblasts from Charcot-Marie-tooth disease type 1A patients. Am. J. Pathol. 188, 728–738.
Li, J., Parker, B., Martyn, C., Natarajan, C., Guo, J., 2013. The PMP22 gene and its related diseases. Mol. Neurobiol. 47, 673–698.
Magyar, J.P., Martini, R., Ruelicke, T., Aguzzi, A., Adlkofer, K., Dembic, Z., Zielasek, J., Toyka, K.V., Suter, U., 1996. Impaired differentiation of Schwann cells in transgenic mice with increased PMP22 gene dosage. J. Neurosci. 16, 5351–5360.
Marques Jr., W., Thomas, P.K., Sweeney, M.G., Carr, L., Wood, N.W., 1998. Dejerine-Sottas neuropathy and PMP22 point mutations: a new base pair substitution and a possible “hot spot” on Ser72. Ann. Neurol. 43, 680–683.
Martini, R., Fischer, S., Lopez-Vales, R., David, S., 2008. Interactions between Schwann cells and macrophages in injury and inherited demyelinating disease. Glia 56, 1566–1577.
Mathews, E.S., Appel, B., 2016. Cholesterol biosynthesis supports myelin gene expression and axon Ensheathment through modulation of P13K/Akt/mTor Signaling. J. Neurosci. 36, 7628–7639.
Mehlem, A., Hagberg, C.E., Muhl, L., Eriksson, U., Falkevall, A., 2013. Imaging of neutral lipids by oil red O for analyzing the metabolic status in health and disease. Nat. Protoc. 8, 1149–1154.
Misko, A., Ferguson, T., Notterpek, L., 2002. Matrix metalloproteinase mediated degradation of basement membrane proteins in trembler J neuropathy nerves. J. Neurochem. 83, 885–894.
Montani, L., Pereira, J.A., Norrmen, C., Pohl, H.B.F., Tinelli, E., Trotzmuller, M., Figlia, G., Dimas, P., von Niederhausern, B., Schwager, R., Jessberger, S., Semenkovich, C.F., Kofeler, H.C., Suter, U., 2018. De novo fatty acid synthesis by Schwann cells is essential for peripheral nervous system myelination. J. Cell Biol. 217, 1353–1368.
Navon, R., Seifried, B., Gal-On, N.S., Sadeh, M., 1996. A new point mutation affecting the fourth transmembrane domain of PMP22 results in severe de novo Charcot-Marie-Tooth disease. Hum. Genet. 97, 685–687.
Nobbio, L., Vigo, T., Abbruzzese, M., Levi, G., Brancolini, C., Mantero, S., Grandis, M., Benedetti, L., Mancardi, G., Schenone, A., 2004. Impairment of PMP22 transgenic Schwann cells differentiation in culture: implications for Charcot-Marie-Tooth type 1A disease. Neurobiol. Dis. 16, 263–273.
Norrmen, C., Figlia, G., Lebrun-Julien, F., Pereira, J.A., Trotzmuller, M., Kofeler, H.C., Rantanen, V., Wessig, C., van Deijk, A.L., Smit, A.B., Verheijen, M.H., Ruegg, M.A., Hall, M.N., Suter, U., 2014. mTORC1 controls PNS myelination along the mTORC1-RXRgamma-SREBP-lipid biosynthesis axis in Schwann cells. Cell Rep. 9, 646–660.
Notterpek, L., Tolwani, R.J., 1999. Experimental models of peripheral neuropathies. Lab. Anim. Sci. 49, 588–599.
Notterpek, L., Shooter, E.M., Snipes, G.J., 1997. Upregulation of the endosomal-lysosomal pathway in the trembler-J neuropathy. J. Neurosci. 17, 4190–4200.
Numakura, C., Lin, C., Oka, N., Akiguchi, I., Hayasaka, K., 2000. Hemizygous mutation of the peripheral myelin protein 22 gene associated with Charcot-Marie-Tooth disease type 1. Ann. Neurol. 47, 101–103.
Ohnishi, A., Yamamoto, T., Izawa, K., Yamamori, S., Takahashi, K., Mega, H., Jinnai, K., 2000. Dejerine-sottas disease with a novel de novo dominant mutation, Ser 149 Arg, of the peripheral myelin protein 22. Acta Neuropathol. 99, 327–330.
Parman, Y., Plante-Bordeneuve, V., Guiochon-Mantel, A., Eraksoy, M., Said, G., 1999. Recessive inheritance of a new point mutation of the PMP22 gene in Dejerine-Sottas disease. Ann. Neurol. 45, 518–522.
Pertusa, M., Morenilla-Palao, C., Carteron, C., Viana, F., Cabedo, H., 2007. Transcriptional control of cholesterol biosynthesis in Schwann cells by axonal neuregulin 1. J. Biol. Chem. 282, 28768–28778.
Rawlins, F.A., Villegas, G.M., Hedley-Whyte, E.T., Uzman, B.G., 1972. Fine structural localization of cholesterol-1,2- 3 H in degenerating and regenerating mouse sciatic nerve. J. Cell Biol. 52, 615–625.
Saher, G., Brugger, B., Lappe-Siefke, C., Mobius, W., Tozawa, R., Wehr, M.C., Wieland, F., Ishibashi, S., Nave, K.A., 2005. High cholesterol level is essential for myelin membrane growth. Nat. Neurosci. 8, 468–475.
Saher, G., Quintes, S., Mobius, W., Wehr, M.C., Kramer-Albers, E.M., Brugger, B., Nave, K.A., 2009. Cholesterol regulates the endoplasmic reticulum exit of the major membrane protein P0 required for peripheral myelin compaction. J. Neurosci. 29, 6094–6104.
Saher, G., Rudolphi, F., Corthals, K., Ruhwedel, T., Schmidt, K.F., Lowel, S., Dibaj, P., Barrette, B., Mobius, W., Nave, K.A., 2012. Therapy of Pelizaeus-Merzbacher disease in mice by feeding a cholesterol-enriched diet. Nat. Med. 18, 1130–1135.
Schmitt, S., Castelvetri, L.C., Simons, M., 2015. Metabolism and functions of lipids in myelin. Biochim. Biophys. Acta 1851, 999–1005.
Scholzen, T., Gerdes, J., 2000. The Ki-67 protein: from the known and the unknown. J. Cell. Physiol. 182, 311–322.
Scurry, A.N., Heredia, D.J., Feng, C.Y., Gephart, G.B., Hennig, G.W., Gould, T.W., 2016. Structural and functional abnormalities of the neuromuscular junction in the trembler-J homozygote mouse model of congenital Hypomyelinating neuropathy. J. Neuropathol. Exp. Neurol. 75, 334–346.
Sedzik, J., Jastrzebski, J.P., Ikenaka, K., 2013. Sequence motifs of myelin membrane proteins: towards the molecular basis of diseases. J. Neurosci. Res. 91, 479–493.
Shy, M.E., Shi, Y., Wrabetz, L., Kamholz, J., Scherer, S.S., 1996. Axon-Schwann cell interactions regulate the expression of c-jun in Schwann cells. J. Neurosci. Res. 43, 511–525.
Suter, U., Moskow, J.J., Welcher, A.A., Snipes, G.J., Kosaras, B., Sidman, R.L., Buchberg, A.M., Shooter, E.M., 1992a. A leucine-to-proline mutation in the putative first transmembrane domain of the 22-kDa peripheral myelin protein in the trembler-J mouse. Proc. Natl. Acad. Sci. U. S. A. 89, 4382–4386.
Suter, U., Welcher, A.A., Ozcelik, T., Snipes, G.J., Kosaras, B., Francke, U., Billings-Gagliardi, S., Sidman, R.L., Shooter, E.M., 1992b. Trembler mouse carries a point mutation in a myelin gene. Nature 356, 241–244.
Tobler, A.R., Notterpek, L., Naef, R., Taylor, V., Suter, U., Shooter, E.M., 1999. Transport of Trembler-J mutant peripheral myelin protein 22 is blocked in the intermediate compartment and affects the transport of the wild-type protein by direct interaction. J. Neurosci. 19, 2027–2036.
Vance, J.E., Hayashi, H., 2010. Formation and function of apolipoprotein E-containing lipoproteins in the nervous system. Biochim. Biophys. Acta 1801, 806–818.
Verheijen, M.H., Chrast, R., Burrola, P., Lemke, G., 2003. Local regulation of fat metabolism in peripheral nerves. Genes Dev. 17, 2450–2464.
Vigo, T., Nobbio, L., Hummelen, P.V., Abbruzzese, M., Mancardi, G., Verpoorten, N., Verhoeven, K., Sereda, M.W., Nave, K.A., Timmerman, V., Schenone, A., 2005. Experimental Charcot-Marie-Tooth type 1A: a cDNA microarrays analysis. Mol. Cell. Neurosci. 28, 703–714.
Werner, H.B., Kramer-Albers, E.M., Strenzke, N., Saher, G., Tenzer, S., Ohno-Iwashita, Y., De Monasterio-Schrader, P., Mobius, W., Moser, T., Griffiths, I.R., Nave, K.A., 2013. A critical role for the cholesterol-associated proteolipids PLP and M6B in myelination of the central nervous system. Glia 61, 567–586.
White, F.V., Toews, A.D., Goodrum, J.F., Novicki, D.L., Bouldin, T.W., Morell, P., 1989. Lipid metabolism during early stages of Wallerian degeneration in the rat sciatic nerve. J. Neurochem. 52, 1085–1092.
Xu, L., Tang, D., Guan, M., Xie, C., Xue, Y., 2014. Effect of high-fat diet on peripheral neuropathy in C57BL/6 mice. Int. J. Endocrinol. 2014, 305205.
Yao, J.K., Dyck, P.J., 1981. Lipid abnormalities in hereditary neuropathy. Part 4. Endoneurial and liver lipids of HMSN-III (Dejerine-Sottas disease). J. Neurol. Sci. 52, 179–190.
Zhou, Y., Miles, J.R., Tavori, H., Lin, M., Khoshbouei, H., Borchelt, D., Bazick, H., Landreth, G.E., Lee, S., Fazio, S., Notterpek, L., 2019. PMP22 regulates cholesterol trafficking and ABCA1-mediated cholesterol efflux. J. Neurosci. 39 (27), 5404–5418.